Quantum tunneling and level crossings in the squeeze-driven Kerr oscillator

Miguel A. Prado Reynoso,[1] D. J. Nader,[2] Jorge Chávez-Carlos,[1] B. E. Ordaz-Mendoza,[1] Rodrigo G. Cortiñas,[3] Victor S. Batista,[4] S. Lerma-Hernández,[5] Francisco Pérez-Bernal,[6,*] and Lea F. Santos[1]

[1]*Department of Physics, University of Connecticut, Storrs, Connecticut 06269, USA*
[2]*Department of Chemistry, Brown University, Providence, Rhode Island 02912, USA*
[3]*Department of Applied Physics and Physics, Yale University, New Haven, Connecticut 06520, USA*
[4]*Department of Chemistry, Yale University, P.O. Box 208107, New Haven, Connecticut 06520-8107, USA*
[5]*Facultad de Física, Universidad Veracruzana, Campus Arco Sur, Paseo 112, C.P. 91097 Xalapa, Mexico*
[6]*Departamento de Ciencias Integradas and Centro de Estudios Avanzados en Física, Matemáticas y Computación, Universidad de Huelva, Huelva 21071, Spain*

(Received 23 May 2023; accepted 25 August 2023; published 13 September 2023)

The quasienergy spectrum recently measured in experiments with a squeeze-driven superconducting Kerr oscillator showed good agreement with the energy spectrum of its corresponding static effective Hamiltonian. The experiments also demonstrated that the dynamics of low-energy states can be explained with the same emergent static effective model. The spectrum exhibits real (avoided) level crossings for specific values of the Hamiltonian parameters, which can then be chosen to suppress (enhance) quantum tunneling. Here we analyze the spectrum and the dynamics of the effective model up to high energies, which should soon be within experimental reach. We show that the parameter values for the crossings, which can be obtained from a semiclassical approach, can also be identified directly from the dynamics. Our analysis of quantum tunneling is done with the effective flux of the Husimi volume of the evolved states between different regions of the phase space. Both initial coherent states and quench dynamics are considered. We argue that the level crossings and their consequences on the dynamics are typical to any quantum system with one degree of freedom, whose density of states presents a local logarithmic divergence and a local step discontinuity.

DOI: 10.1103/PhysRevA.108.033709

I. INTRODUCTION

Tunneling is a quantum-mechanical phenomenon in which a system evolves through an energy barrier that it cannot penetrate classically. In the 1920s, tunneling successfully explained molecular spectral features [1,2], electron emission from metals [3], and α decay from nuclei [4,5]. Tunneling through inversion or internal rotation is deemed responsible for the details associated with high-resolution molecular spectroscopy of equivalent conformers [6]. A well-known example is the tunneling in the ground state of the ammonia molecule [6,7], whose associated energy splitting was used in the first maser, pedagogically explained in [8]. Tunneling is also of major importance to understand chemical reaction rates, though the modeling of chemical reactions where tunneling plays a vital role is hampered by the high dimensionality of the systems involved and experimental difficulties [9,10]. A recent work was able to find fine agreement between *ab initio* calculations and experimental results for the tunneling reaction of hydrogen molecules with deuterium anions [11]. There are several other observed examples of tunneling, such as in experiments involving atomic systems [12], superconducting circuits [13,14], and NMR techniques [15].

The literature is particularly vast for quantum tunneling in double-well systems [16–28], as in experiments with superconducting circuits [29]. Of particular interest to us is the case of driven oscillators with period-doubling bifurcations [16–21], whose static effective Hamiltonians represent double-well systems. Experimentally, this was recently achieved in the quantum regime by applying a microwave drive to a superconducting nonlinear asymmetric inductive element [30] transmon. The static effective Hamiltonian of this system corresponds to a squeeze-driven Kerr oscillator, where the squeezing amplitude and the detuning of the drive control the energy barrier of a double well [31]. The implementation of a double-well system has the advantage of allowing *in situ* tunability of all its Hamiltonian parameters and demonstrated access to the excited states [31], properties that we exploit in this work. Some of the dynamical properties of this system, which includes the exponential growth of the out-of-time-ordered correlator due to instability [32], were investigated in Ref. [33]. Tunneling in the squeeze-driven Kerr oscillator was recently observed experimentally for the few lowest excited states in Refs. [30,34]. Here we extend this study to higher energies.

The energy spectrum of the squeeze-driven Kerr oscillator presents real and avoided energy crossings for specific values of the Hamiltonian parameters [34]. They appear when the ratio Δ/K between the frequency Δ of the harmonic part of the Hamiltonian and the Kerr amplitude K is an integer

*Also at Instituto Carlos I de Física Teórica y Computacional, Universidad de Granada, Fuentenueva s/n, 18071 Granada, Spain.

number [34]. A similar behavior was theoretically predicted for the Lipkin-Meshkov-Glick model [28]. Both systems have one degree of freedom, conserve parity, and are described by double wells. The crossings are real when the states have different parity, in which case tunneling is suppressed, and they are avoided for states with the same parity, leading to maximum tunneling.

In Sec. II we provide a detailed analysis of the Hamiltonian of the squeeze-driven Kerr oscillator and employ semiclassical phase-space methods to elucidate the origin of the crossings. The values of the Hamiltonian parameters at which the crossings occur are determined via a semiclassical approach based on the Einstein-Brillouin-Keller quantization rule [35–37], as discussed in Refs. [28,34,38] (see also how to associate the crossings with the existence of a quasispin symmetry in [39]). We argue that these results are general to systems with one degree of freedom whose density of states (DOS) exhibits a local logarithmic divergence and a local step discontinuity.

In Sec. III we use the effective flux of the Husimi volume to monitor the spread of an evolved state into specific regions of phase space that are classically forbidden. We explore two scenarios, one where the dynamics is initiated with a coherent state and the other where a Hamiltonian parameter is quenched. The tunneling amplitude changes depending on the ratio Δ/K, decreasing (increasing) for values of Δ/K associated with real (avoided) crossings. We show that the locations of the energy crossings can be dynamically identified.

II. MODEL, EIGENVALUES, AND EIGENSTATES

The static effective Hamiltonian that describes the considered Kerr oscillator under a squeezing drive is written as [31,34]

$$\hat{H} = -\Delta\hat{a}^\dagger\hat{a} + K\hat{a}^{\dagger 2}\hat{a}^2 - \epsilon_2(\hat{a}^{\dagger 2} + \hat{a}^2), \tag{1}$$

where $\hat{a}^\dagger$ and $\hat{a}$ are the bosonic creation and annihilation operators, respectively, the amplitude Δ of the harmonic part of the Hamiltonian is the detuning between the frequency of the oscillator and half frequency of the drive, K is the amplitude of the Kerr nonlinearity, ϵ_2 is the squeezing amplitude, and we set $\hbar = 1$. The Hamiltonian (1) conserves parity, that is, $[\hat{H},\hat{\mathcal{P}}] = 0$, where the parity operator $\hat{\mathcal{P}} = e^{-i\pi\hat{n}} = (-1)^{\hat{n}}$. We refer to the parity as either negative or positive. The notation for the eigenstates and eigenvalues is $\hat{H}|\psi_k\rangle = E_k|\psi_k\rangle$.

The effective model in Eq. (1) is valid not only for small detuning values. Indeed, the experiments have so far reached $\Delta/K \sim 14$ and the model has remained valid. The experimental effective Hamiltonian in Ref. [34] has an overall negative sign with respect to ours, $-\hat{H}$. We choose to write it as in Eq. (1) for convenience, so we have wells instead of hills. In what follows, we take $\epsilon_2 > 0$.

The Hamiltonian in Eq. (1) is unbounded. We choose values for the size N of the truncated Hilbert space that guarantee the convergence of the eigenvalues and eigenstates under study. This unbounded Hamiltonian exhibits several properties similar to those of the bounded Lipkin-Meshkov-Glick Hamiltonian studied in [28]. They include the presence of a quantum phase transition (QPT), one or two excited-state quantum phase transitions (ESQPTs) [40–42], and real and avoided energy level crossings, which are the focus of this paper.

We note that the static effective model in Eq. (1) ceases to describe the system when the drive becomes sufficiently strong. This is due to the emergence of chaos [43], which, as the amplitude of the drive increases, sets in first among the high energies. The use of superconducting circuits to investigate the onset of quantum chaos and its dynamical consequences is beyond the scope of the present work.

A. Classical limit and stationary points

We gain insight into the system described by Eq. (1) by examining the classical limit [33,34] of the Hamiltonian in the canonical variables q and p, which reads

$$H_{\rm cl} = -\frac{\Delta}{2}(q^2+p^2) + \frac{K}{4}(q^2+p^2)^2 - \epsilon_2(q^2-p^2). \tag{2}$$

The classical energy for a point (q, p) in phase space is defined as $\mathcal{E} = H_{\rm cl}(q, p)$.

The first important step in our study of the classical Hamiltonian system is the identification of its stationary (critical) points. For the classical Hamiltonian (2), the Hamilton's equations of motion are

$$\begin{aligned} \dot{q} &= -p[\Delta - K(q^2+p^2) - 2\epsilon_2], \\ \dot{p} &= q[\Delta - K(q^2+p^2) + 2\epsilon_2]. \end{aligned} \tag{3}$$

At the critical points we have that $\dot{q} = 0$ and $\dot{p} = 0$. Solving the system of equations above, we distinguish five critical points $r = \{q, p\}$, which are listed below together with their corresponding energy $\mathcal{E}$:

$$\begin{aligned} &r_0 = \{0, 0\}, \quad \mathcal{E}_{r_0} = 0, \\ &r_1^\pm = \left\{0, \pm\sqrt{\frac{\Delta - 2\epsilon_2}{K}}\right\}, \quad \mathcal{E}_{r_1^\pm} = -\frac{(\Delta-2\epsilon_2)^2}{4K}, \\ &r_2^\pm = \left\{\pm\sqrt{\frac{\Delta + 2\epsilon_2}{K}}, 0\right\}, \quad \mathcal{E}_{r_2^\pm} = -\frac{(\Delta+2\epsilon_2)^2}{4K}. \end{aligned} \tag{4}$$

By analyzing the stability of these points, we identify the following three scenarios [28,34].

Case I. For $\Delta/K \leqslant -2\epsilon_2/K$, there is only one stationary point at r_0, as shown in the phase-space diagram of Fig. 1(a) (brown star). This stable point is a global minimum.

Case II. For $-2\epsilon_2/K < \Delta/K \leqslant 2\epsilon_2/K$, there are three stationary points, as shown in the phase-space diagram of Fig. 1(b). Two of them are stable points at $r_2^\pm$, which are global minima (brown stars), and r_0 now becomes an unstable hyperbolic point (red star).

Case III. For $\Delta/K > 2\epsilon_2/K$, there are five stationary points, as shown in the phase-space diagram of Fig. 1(c). These are the same two stable global minima at $r_2^\pm$ (brown stars) as in case II, there are also two unstable hyperbolic points at $r_1^\pm$ (red stars), and r_0 recovers its status of a stable point, as in case I, though now it is a local maximum (blue star).

Figure 1(d) depicts the parameter space of the classical Hamiltonian in Eq. (2), classified in accordance with the three types of phase-space diagrams discussed above.

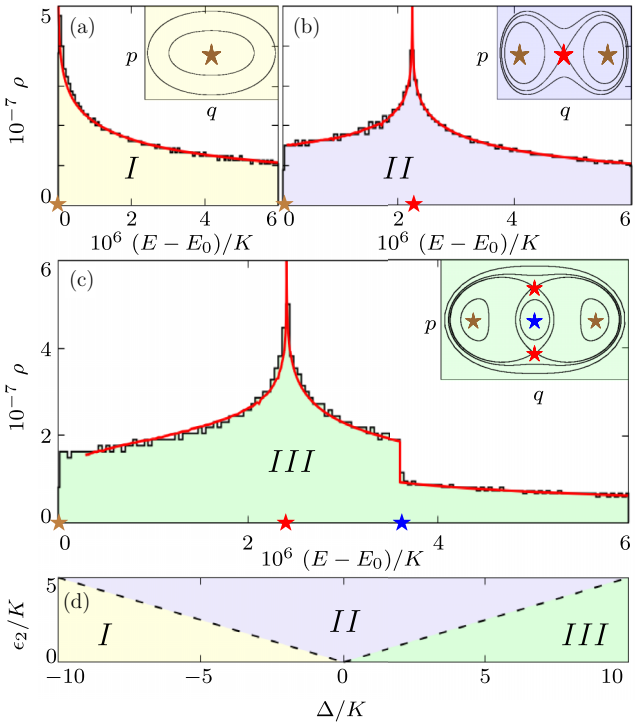

FIG. 1. (a)–(c) Density of states calculated by exact numerical diagonalization, with the insets showing phase-space diagrams, and (d) parameter space for regions I, II, and III. The red solid line in (a)–(c) indicates the semiclassical approximation of the DOS. The critical points of the phase-space diagrams in the insets and their energies in (a)–(c) are marked with stars: brown for minimum energy, red for unstable hyperbolic points, and blue for a local maximum. The DOS exhibits a peak in (b) for case II at $E^{(\mathrm{II})}_{\mathrm{ESQPT}}$ (red star) and in (c) both a peak at $E^{(\mathrm{III})}_{\mathrm{ESQPT}}$ (red star) and a step discontinuity at $E^{(\mathrm{III})}_{\mathrm{step}}$ (blue star) for case III. For case I in (a), $\Delta/K=-3000$ and $\epsilon_2/K=400$; for case II in (b) $\Delta/K=0$ and $\epsilon_2/K=1500$; and for case III in (c), $\Delta/K=3000$ and $\epsilon_2/K=400$. The DOS includes both parities and is normalized considering the energy interval $E-E_0\in[0,6\times10^6]$. The size of the truncated Hilbert space is $N=2000$ for each parity sector.

B. Density of states

The DOS obtained with the eigenvalues E_k of the Hamiltonian in Eq. (1) detects excited-state quantum phase transitions associated with bifurcations [21] in the classical phase space [41,42], as we describe in this section. Figures 1(a)–1(c) present the DOS as a function of the excitation energy $E'=E-E_0$, where E_0 is the ground-state energy. The shape of the DOS can also be reproduced from the semiclassical approximation

$$\rho(\mathcal{E})=\frac{1}{2\pi}\int dq\,dp\,\delta(H_{\mathrm{cl}}-\mathcal{E}), \tag{5}$$

where H_{cl} is the classical Hamiltonian in Eq. (2), and the result for Eq. (5) is obtained using the lowest-order term of the Gutzwiller trace formula [44]. This result is shown with a red line in Figs. 1(a)–1(c). Each one of the three cases identified in Sec. II A is characterized by a different structure of the DOS, as follows.

For case I in Fig. 1(a), the DOS decays monotonically as energy increases. A QPT happens at $\Delta/K=-2\epsilon_2/K$. This transition was studied in [45] and can be understood from the analysis of the stationary points. As Δ/K grows from $-\infty$ and reaches $\Delta/K=-2\epsilon_2/K$, the single stationary point at r_0 duplicates into $r_2^{\pm}$. This implies that, in the quantum domain, the energy difference between the ground state and the first excited state vanishes exponentially due to tunneling.

For case II in Fig. 1(b), the DOS exhibits a peak at the energy denoted by $E^{(\mathrm{II})}_{\mathrm{ESQPT}}$ (red star), which converges to the energy of the unstable critical point r_0 in the classical limit,

$$E'^{(\mathrm{II})}_{\mathrm{ESQPT}}\to\mathcal{E}_{r_0}-\mathcal{E}_{r_2^{\pm}}=\frac{(\Delta+2\epsilon_2)^2}{4K}. \tag{6}$$

This accumulation of eigenvalues around $E'^{(\mathrm{II})}_{\mathrm{ESQPT}}$ diverges as we approach the classical limit and is the main signature of what has become known as the ESQPT [40,42]. The ESQPT critical energy value marks the boundary between two regions with different dominating symmetries. Pairs of eigenvalues, one with negative parity and the other with positive parity, are degenerate for energies below the ESQPT energy and they split once they get above the ESQPT energy [33].

For case III in Fig. 1(c), the DOS exhibits two distinct nonanalytical features: a logarithmic peak and a discontinuous step. The peak is associated with the hyperbolic points (red stars in the inset) in the classical phase space and characterizes a first ESQPT. It happens at the energy $E^{(\mathrm{III})}_{\mathrm{ESQPT}}$ (red star in the main panel), which converges to the energy of the unstable critical points $r_2^{\pm}$ in the classical limit. Therefore, the excitation energy is given by

$$E'^{(\mathrm{III})}_{\mathrm{ESQPT}}\to\mathcal{E}_{r_1^{\pm}}-\mathcal{E}_{r_2^{\pm}}=\frac{2\Delta\epsilon_2}{K}. \tag{7}$$

The discontinuous step happens at an energy that converges to the energy of the local maximum (blue star in the inset) at the origin of the classical phase space,

$$E'^{(\mathrm{III})}_{\mathrm{step}}\to\mathcal{E}_{r_0}-\mathcal{E}_{r_2^{\pm}}=\frac{(\Delta+2\epsilon_2)^2}{4K}. \tag{8}$$

The discontinuity at the energy $E^{(\mathrm{III})}_{\mathrm{step}}$ (blue star in the main panel) characterizes a second kind of ESQPT.

The dynamical consequences of the presence of the ESQPT in case II for $\Delta=0$ were studied in [33]. In the present work we focus on case III, where $\Delta/K>2\epsilon_2/K$ and two ESQPTs exist, one associated with the two hyperbolic points and the other with the local maximum.

C. Avoided and real level crossings

We now fix a value of ϵ_2/K and calculate the spectrum of the Hamiltonian (1) as a function of Δ/K for case III. However, before presenting these results, it is informative to analyze the trajectories of the underlying classical system (2).

Recall that the classical phase space of case III has a local maximum at $r_0=\{0,0\}$ with energy $\mathcal{E}_{r_0}=0$. The trajectories with energy less than $\mathcal{E}_{r_0}$ are degenerate in pairs, that is, there are two trajectories with the same energy. These pairs of trajectories can be distinguished depending on the region of the phase space where they occur. One type belongs to the left and right regions of the phase space denoted by Ω_{l} and Ω_{r},

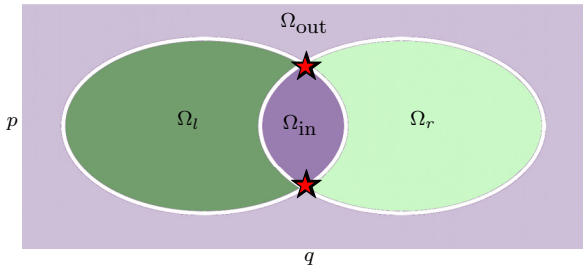

FIG. 2. Sketch of the classical phase space for case III separated in regions defined by the separatrix (white color) of the first ESQPT, which is associated with the hyperbolic points (red stars). The regions $\Omega_{\rm l}$ and $\Omega_{\rm r}$ (green areas) contain pairs of degenerate classical trajectories with energies below the energy of the first ESQPT, $\mathcal{E} < E^{\rm (III)}_{\rm ESQPT}$. The regions $\Omega_{\rm in}$ and $\Omega_{\rm out}$ (purple areas) contain pairs of degenerate classical trajectories with energies between the first and second ESQPTs, $E^{\rm (III)}_{\rm ESQPT} < \mathcal{E} < E^{\rm (III)}_{\rm step}$.

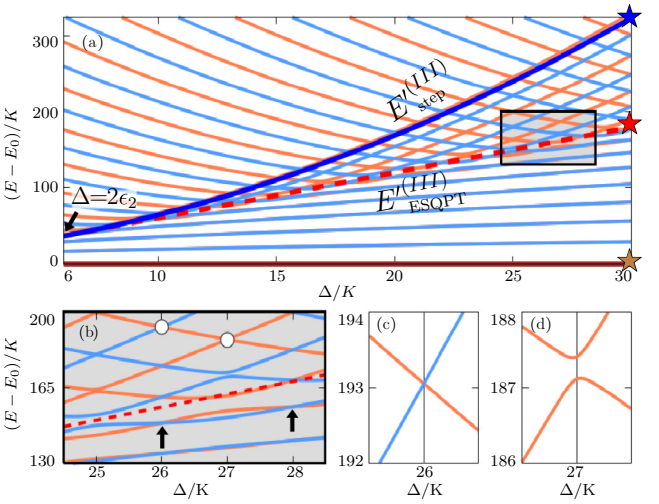

FIG. 3. Excitation energy spectrum as a function of the control parameter Δ/K for fixed $\epsilon_2/K = 3$ and $\Delta/K \geqslant 2\epsilon_2/K$. The plot corresponds to case III, where two ESQPTs exist [cf. Fig. 1(c)]. Orange (blue) lines indicate the levels in the positive (negative) parity sector. The red dashed line in (a) and (b) marks the energy $E'^{(\rm III)}_{\rm ESQPT}$ of the first ESQPT and the dark blue line in (a) corresponds to the energy $E'^{(\rm III)}_{\rm step}$ of the second ESQPT. The small rectangle in (a) is amplified in (b). In the latter, the vertical arrows at $\Delta/K = 26$ and 28 mark points where the degeneracy is not lifted as one approaches $E'^{(\rm III)}_{\rm ESQPT}$ from below, the circle at $\Delta/K = 26$ indicates a real crossing that is shown again in (c), and the circle at $\Delta/K = 27$ corresponds to an avoided crossing, which is evinced in (d).

respectively, in Fig. 2. The other type is found in the $\Omega_{\rm in}$-$\Omega_{\rm out}$ regions of Fig. 2. These two types of trajectory pairs manifest differently in the quantum model, as described below.

(i) The $\Omega_{\rm l}$-$\Omega_{\rm r}$ region depicted in green in Fig. 2 contains pairs of degenerate trajectories with energy $\mathcal{E}$ less than the energy of the hyperbolic point,

$$\mathcal{E} < \mathcal{E}_{r_{\rm l}^{\pm}} \simeq E^{\rm (III)}_{\rm ESQPT}.$$

Each trajectory of the degenerate pair is located in one of the two wells centered at the global minima at $r_2^{\pm}$, with each one being the reflection on the q axis of the other one.

(ii) The $\Omega_{\rm in}$-$\Omega_{\rm out}$ region depicted in purple in Fig. 2 contains pairs of degenerate trajectories that have energy $\mathcal{E}$ between the energy of the hyperbolic points and the local maximum,

$$E^{\rm (III)}_{\rm ESQPT} \simeq \mathcal{E}_{r_{\rm i}^{\pm}} < \mathcal{E} < \mathcal{E}_{r_0} \simeq E^{\rm (III)}_{\rm step}.$$

For this region, contrary to what happens in the $\Omega_{\rm l}$-$\Omega_{\rm r}$ region, the size of the phase-space area covered by each trajectory of the degenerate pair is different, the one in $\Omega_{\rm in}$ being smaller than the one in $\Omega_{\rm out}$.

We are now in a position to further analyze the spectrum of the Hamiltonian (1) for case III. In Fig. 3 we set $\epsilon_2/K = 3$ and show the eigenvalues as a function of Δ/K. The results belong to case III, because the levels are shown for $\Delta/K > 6$. The orange (blue) lines correspond to the energies in the positive (negative) parity sector. The red dashed line marks the first-ESQPT energy $E'^{(\rm III)}_{\rm ESQPT}$ [see Eq. (7)] and the dark blue line shows the energy of the second ESQPT, associated with the discontinuous step $E'^{(\rm III)}_{\rm step}$ [see Eq. (8)].

Considering Fig. 3(a), we can better understand the features of the DOS observed in Fig. 1(c) and extract further details, as described next.

(i) For $E' < E'^{(\rm III)}_{\rm ESQPT}$ [below the red dashed line in Fig. 3(a)], the spectrum is exponentially quasidegenerate in pairs (kissing) for any value of Δ/K. One level of the pair belongs to the positive parity sector and the other one to the negative parity sector, so the blue and orange lines are superposed. Classically, this manifests as pairs of phase-space trajectories with equal energy, where one trajectory belongs to the $\Omega_{\rm l}$ region and the other to the $\Omega_{\rm r}$ region of Fig. 2.

(ii) As one approaches $E' \sim E'^{(\rm III)}_{\rm ESQPT}$ from below, the degeneracy between states of negative and positive parity is lifted throughout, except where Δ/K is even, as indicated with vertical arrows in Fig. 3(b). This is an important region of the spectrum for the analysis of quantum tunneling, as it will be explained in Sec. III B.

(iii) Another special spectral region for this work takes place at energies between the two ESQPTs of case III,

$$E^{\rm (III)}_{\rm ESQPT} < E < E^{\rm (III)}_{\rm step}, \tag{9}$$

that is, between the red dashed and dark blue solid lines in Fig. 3(a). Classically, this energy interval is associated with trajectories in the regions $\Omega_{\rm in}$ and $\Omega_{\rm out}$ of Fig. 2. As seen in Figs. 3(a) and 3(b), there are crossings of energy levels for certain values of the control parameter Δ/K. They happen between energies of different parity sectors when Δ/K is even and between energies within the same parity when Δ/K is odd. From a closer look at Figs. 3(c) and 3(d) and in agreement with the von Neumann–Wigner theorem [46,47], one sees that the crossings for levels of different parities are real, while the crossings for levels of the same parity sector are avoided.

(iv) For $E' > E'^{(\rm III)}_{\rm step}$ [above the dark blue solid line in Fig. 3(a)], the spectrum ceases to present any crossing; the energies simply increase, alternating between positive and negative parity.

Motivated by the analysis in Ref. [28] (see also the Supplemental Material in Ref. [34]), we show that the crossings in the energy region between the two ESQPTs, $E_{\rm ESQPT}^{\rm (III)} < E < E_{\rm step}^{\rm (III)}$, can be explained using a semiclassical approach based on the Einstein-Brillouin-Keller quantization rule,

$$I = \frac{1}{2\pi}\oint p\,dq = \left(n + \frac{\mu}{4} + \frac{b}{2}\right), \tag{10}$$

which applies to nonchaotic systems [37]. In the equation above, I is the action-angle coordinate for our system with one degree of freedom and n is a positive integer. The Maslov indices μ and b indicate the number of classical turning points in the trajectory and the number of reflections with a hard wall, respectively. The trajectories for the Hamiltonian (2) in the regions $\Omega_{\rm in}$ and $\Omega_{\rm out}$ have two turning points, so $\mu = 2$, and no reflection with a hard wall, so $b = 0$.

To solve Eq. (10), we consider a canonical transformation to variables (z, ϕ) defined as $q = \sqrt{2z}\sin\phi$ and $p = \sqrt{2z}\cos\phi$, with ϕ covering the entire interval $\phi = [0, 2\pi)$, and use the classical Hamiltonian in Eq. (2) to write

$$\mathcal{E} = H_{\rm cl}(z, \phi) = Kz^2 + (\gamma - \Delta)z, \tag{11}$$

where $\gamma = 2\epsilon_2\cos(2\phi)$. For $\mathcal{E} \in [\mathcal{E}_{r_2^\pm}, \mathcal{E}_{r_0}]$, the two solutions are

$$z_\pm(\mathcal{E}, \phi) = \frac{\Delta - \gamma \pm \sqrt{(\Delta-\gamma)^2 + 4K\mathcal{E}}}{2K}. \tag{12}$$

Resorting to the Einstein-Brillouin-Keller quantization rule in Eq. (10) in terms of the canonical variables (z and ϕ), we obtain the semiclassical approximation for the energy of each trajectory,

$$\frac{1}{2\pi}\int_0^{2\pi} z_\pm(\mathcal{E}_{n_\pm}, \phi)d\phi = \left(n_\pm + \frac{1}{2}\right), \tag{13}$$

where $\mathcal{E}_{n_\pm}$ are the semiclassical energies and $n_\pm$ are integer numbers. If the energy levels are degenerate, $\mathcal{E}_{n_+} = \mathcal{E}_{n_-}$, then Eq. (13) gives

$$\frac{1}{2\pi}\int_0^{2\pi}(z_+ + z_-)d\phi = \frac{\Delta}{K} = (n_+ + n_- + 1),$$

which implies that

$$\frac{\Delta}{K} = n_+ + n_- + 1. \tag{14}$$

From this semiclassical approach, we conclude that there are crossings whenever Δ/K is an integer, although it is not possible to say whether the crossings are real or avoided. The distinction between the two is made in this work with the numerical diagonalization, as shown in Fig. 3 (see also [34,39]), and they follow the von Neumann–Wigner theorem.

Concisely, the semiclassical approximation reveals that the degeneracies below the first ESQPT (below $E_{\rm ESQPT}^{\rm (III)}$) and the crossings between the two ESQPTs (between $E_{\rm ESQPT}^{\rm (III)}$ and $E_{\rm step}^{\rm (III)}$) are a consequence of the presence of at least two orbits in phase space with the same energy. If these classical orbits enclose identical areas (as in the $\Omega_{\rm l}$ and $\Omega_{\rm r}$ regions), then the corresponding quantum energies are degenerate. If the areas enclosed by two orbits with the same energy are different (as in the $\Omega_{\rm in}$ and $\Omega_{\rm out}$ regions), then the spectrum exhibits crossings for specific values of Δ/K. The crossings are real for levels in different parity sectors and avoided for levels with the same parity.

We conjecture that these crossings in an intermediate-energy region of the spectrum emerge for any system with one degree of freedom, whose DOS is similar to the one for case III seen in Fig. 1(c), that is, the DOS exhibits a local logarithmic divergence and a local step discontinuity, which must be consecutive and can appear in any order. The crossings are expected to appear at energies located between these two ESQPTs. Correspondingly, in the underlying semiclassical system, there should be at least two local stationary points in the phase space, a local hyperbolic point and a local center point, which are related to the logarithmic divergence and the step discontinuity of the DOS, respectively. Other one-body systems that exhibit a similar spectral structure and energy crossings include the one-dimensional asymmetric double-well case [48], the Lipkin-Meshkov-Glick model [28], and the Bose-Hubbard model [49]. The last two correspond to many-body models with all-to-all couplings, which effectively reduces them to one degree of freedom. The analysis of the effects of real and avoided crossings to tunneling in a system with one degree of freedom was also performed in Refs. [17,18], but in this case, the study focused directly on the Floquet spectrum of the driven system.

D. Structure of the eigenstates

The structure of the eigenstates reflects the presence of the real and avoided crossings in the energy interval $E_{\rm ESQPT}^{\rm (III)} < E < E_{\rm step}^{\rm (III)}$ of the spectrum of case III. This can be visualized by inspecting the Husimi functions of the eigenstates. For an eigenstate $|\psi_k\rangle$, the Husimi function

$$\mathcal{Q}_{\psi_k}^{(\alpha)} = \frac{1}{\pi}|\langle\alpha|\psi_k\rangle|^2 = \frac{1}{\pi}\left|\sum_{n=0}^{N-1} c_n^k e^{-|\alpha|^2/2}\frac{\alpha^{*n}}{\sqrt{n!}}\right|^2 \tag{15}$$

is defined as the absolute square of the projection of the eigenstate in the Glauber coherent state

$$|\alpha\rangle = e^{-|\alpha|^2/2}\sum_{n=0}^{N-1}\frac{\alpha^n}{\sqrt{n!}}|n\rangle, \tag{16}$$

where $\hat{a}|\alpha\rangle = \alpha|\alpha\rangle$,

$$\alpha = \sqrt{\tfrac{1}{2}}(q + ip), \tag{17}$$

$|n\rangle$ are the Fock states, $\hat{a}^\dagger\hat{a}|n\rangle = n|n\rangle$, and $c_n^k = \langle n|\psi_k\rangle$. The Husimi function provides a picture of the eigenstate in phase space, thus connecting the structure of the state with the different phase-space regions identified in Fig. 2.

In Fig. 4 we choose an odd value of Δ/K (left column) and an even value of Δ/K (right column) and show the Husimi functions for five eigenstates $|\psi_k\rangle$ with energy immediately above the energy of the first ESQPT. The value of ϵ_2/K is kept fixed. The energies of the eigenstates coincide with those of trajectories in the $\Omega_{\rm in}$ and $\Omega_{\rm out}$ regions of the phase space depicted in Fig. 2. The Husimi function in Fig. 4 is shown in orange for odd Δ/K, where avoided crossings occur, and in blue for even Δ/K, where real crossings occur. Brighter

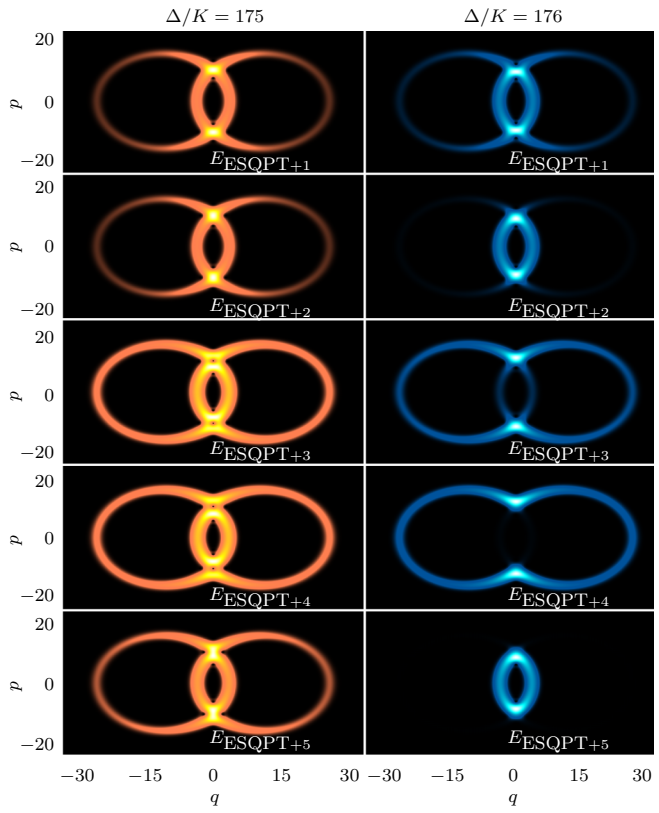

FIG. 4. Husimi function of eigenstates with energy immediately above the ESQPT for $\Delta/K = 175$ (left column) and $\Delta/K = 176$ (right column). Brighter tones of orange (left) or blue (right) indicate larger values of the Husimi function. In all panels $\epsilon_2/K = 50$.

tones of orange or blue indicate larger values of the Husimi function. For the odd Δ/K, the Husimi function lies in both regions Ω_{in} and Ω_{out}. In contrast, for the even Δ/K, the Husimi function is only different from zero either in Ω_{in} or in Ω_{out}, as evident from Figs. 3(c) and 3(d). (When the energy is very close to $E^{(\text{III})}_{\text{ESQPT}}$, despite Δ/K being even, the Husimi function in the three top panels on the right in Fig. 4 is predominantly in one of the two regions Ω_{in} or Ω_{out} but has a small probability to be found in the other one.)

In addition to the Husimi functions, we compute the participation ratio of the eigenstates written in the Fock basis, $|\psi_k\rangle = \sum_n c_n^k |n\rangle$. This quantity is defined as

$$P_R^{(k)} = \left(\sum_{n=0}^{N-1} |\langle n|\psi_k\rangle|^4 \right)^{-1}. \tag{18}$$

It measures the level of delocalization of the state in a chosen basis. The participation ratio is large for an extended state and small for a localized state.

In Fig. 5 we show the participation ratio for eigenstates in a broad interval of energy, which in addition to the region of crossings includes also energies smaller than $E^{(\text{III})}_{\text{ESQPT}}$ and larger than $E^{(\text{III})}_{\text{step}}$. This allows for a parallel between the features of the full spectrum of case III and the level of delocalization of its eigenstates. For fixed $\epsilon_2/K = 50$, an odd value of Δ/K is used for Fig. 5(a) and an even value for Fig. 5(b). In each panel, the points have two different colors,

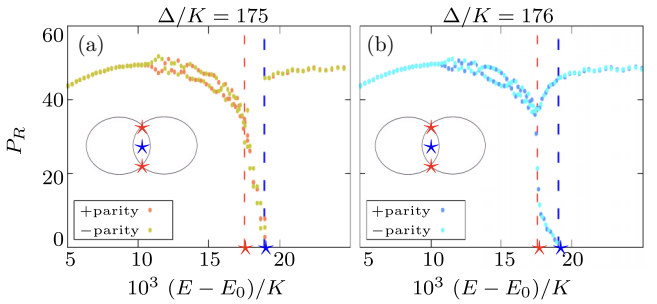

FIG. 5. Participation ratio in the Fock basis for (a) $\Delta/K = 175$ and (b) $\Delta/K = 176$. The vertical red dashed line indicates the energy of the first ESQPT (peak in Fig. 1) and the vertical blue dashed line marks the local maximum energy of the second ESQPT (discontinuous step in Fig. 1). Colors (a) orange and (b) blue correspond to the positive parity and (a) yellow and (b) cyan to the negative parity. In both panels $\epsilon_2/K = 50$.

one for the positive parity and the other for the negative parity. In both panels, the vertical red dashed line marks the energy of the first ESQPT, $E^{(\text{III})}_{\text{ESQPT}}$, and the vertical blue dashed line represents the energy of the second ESQPT at $E^{(\text{III})}_{\text{step}}$ (see Fig. 1).

Below the first ESQPT, the behavior of the participation ratio in both Figs. 5(a) and 5(b) is equivalent: It first grows as the energy increases and then starts decaying at the same time that a peculiar interlace pattern in the participation ratio appears as one approaches $E^{(\text{III})}_{\text{ESQPT}}$.[1] The results in both panels are also analogous for energies above $E^{(\text{III})}_{\text{step}}$, in which case the participation ratio simply grows as the energy increases.

The distinction between Figs. 5(a) and 5(b) happens in the region of the spectrum where the crossings emerge, for $E^{(\text{III})}_{\text{ESQPT}} < E < E^{(\text{III})}_{\text{step}}$. When Δ/K is odd (avoided crossings), one sees in Fig. 5(a) that the participation ratio decays monotonically as one approaches the local maximum energy at $E^{(\text{III})}_{\text{step}}$. Recall that, classically, this is the energy of the local maximum at r_0. In contrast, for even Δ/K, for which the crossings are real, the participation ratio in Fig. 5(b) splits in two branches. In one ramification, P_R decreases monotonically, corresponding to the eigenstates whose Husimi functions are distributed over classical trajectories in Ω_{in}. In the other branch, P_R grows with E; these are the eigenstates whose Husimi functions lie in Ω_{out}.

III. QUANTUM TUNNELING

In this section we explore the dynamical consequences of the real and avoided crossings of case III. Our focus is on the tunneling phenomenon, which involves the quantum-mechanical motion of an initial state between regions of phase space that are classically forbidden. Our analysis requires a quantity capable of measuring how the evolved state samples specific regions of phase space. This can be done with the Husimi function in the position and momentum representation

[1]The localization of the eigenstate at the ESQPT was studied for this model with $\Delta = 0$ in [33]. A general discussion of this feature for various models was presented before in [50].

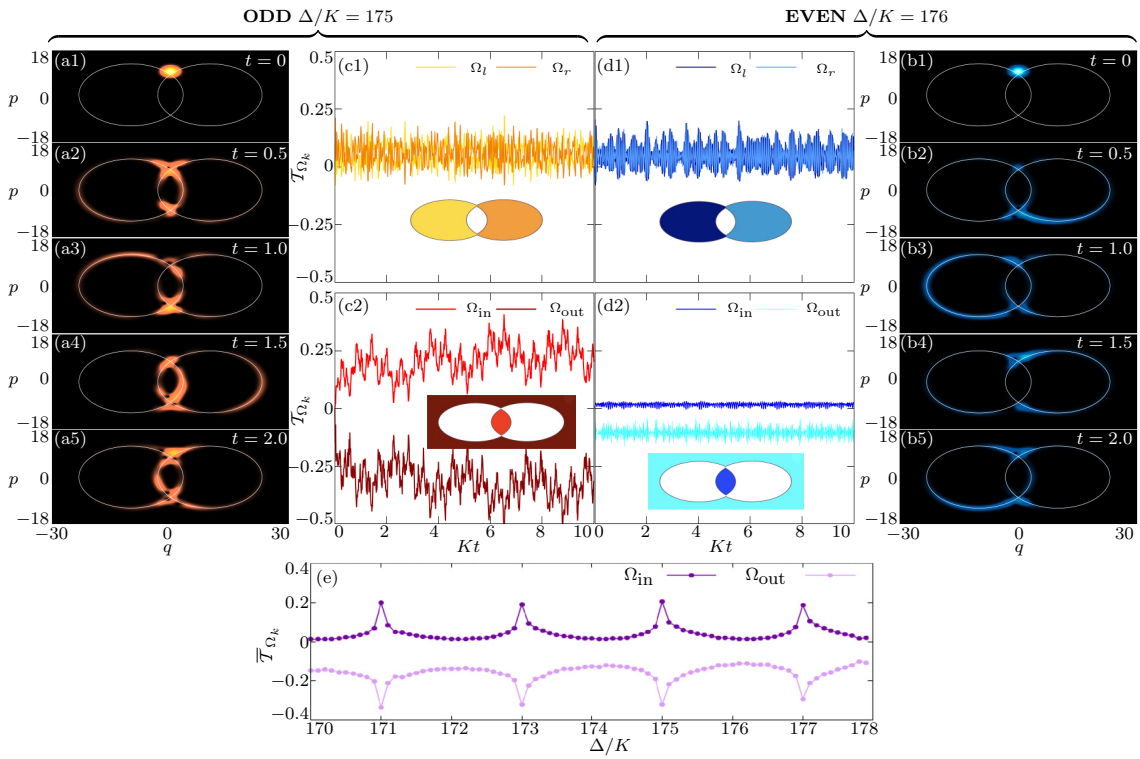

FIG. 6. Evolution of the Husimi function $\mathcal{Q}^{(q,p)}_{\Psi(t)}$ for a coherent state initially centered in the region $\Omega_{\rm out}$ for (a1)–(a5) $\Delta/K = 175$ and (b1)–(b5) $\Delta/K = 176$. The white solid line in these panels indicates the separatrix associated with the hyperbolic fixed points at the energy of the first ESQPT. The energy of the initial coherent state is immediately above the first-ESQPT energy. The results for the effective tunneling $\mathcal{T}_{\Omega_k}$ as a function of dimensionless time are shown in (c1) and (d1) for the regions $\Omega_{\rm l}$ and $\Omega_{\rm r}$ and in (c2) and (d2) for the regions $\Omega_{\rm in}$ and $\Omega_{\rm out}$, for (c1)–(c2) $\Delta/K = 175$ and (d1)–(d2) $\Delta/K = 176$. (e) The mean effective tunneling $\overline{\mathcal{T}_{\Omega_k}(t,0)}$ as a function of the parameter Δ/K is obtained for $Kt \in [0, 10]$. In all panels $\epsilon_2/K = 5$.

now computed for the evolved state $|\Psi(t)\rangle = e^{-i\hat{H}t}|\Psi(0)\rangle$,

$$\mathcal{Q}^{(q,p)}_{\Psi(t)} = \frac{1}{\pi}|\langle\alpha(q,p)|\Psi(t)\rangle|^2, \tag{19}$$

instead of for eigenstates, as in Eq. (15).

In the following we describe our method for capturing quantum tunneling to specific regions of phase space. Given a phase space $\mathcal{M}$, let us first define the invariant regions Ω in which we are interested in studying tunneling dynamics. We say that a region $\Omega \subset \mathcal{M}$ is invariant if for any initial condition $x \in \Omega$ the classical trajectory stays in that same region Ω, that is, $\varphi_x(t) \in \Omega$ for all t, where $\varphi : \mathbb{R} \times \mathcal{M} \to \mathcal{M}$ is the flow defined by the Hamilton's equations of motion (3). We are interested in the four invariant regions of phase space that are depicted in Fig. 2 corresponding to case III: two regions with energy below the energy of the first ESQPT, $\Omega_{\rm l}$ and $\Omega_{\rm r}$, and two regions with energy above the first ESQPT energy, $\Omega_{\rm in}$ and $\Omega_{\rm out}$.

For a particular invariant region in phase space $\Omega_k \subset \mathcal{M}$, we define the Husimi volume at time t as [51]

$$\mathcal{V}_{\Omega_k}(t) = \iint_{\Omega_k} dq\, dp\, \mathcal{Q}^{(q,p)}_{\Psi(t)}, \tag{20}$$

which can be evaluated efficiently by randomly sampling the Husimi function, that is, by Monte Carlo integration [28]. The Husimi volume is normalized, so $\mathcal{V} = 1$ when the integral in Eq. (20) is done over the whole phase space $\Omega_k = \Omega$.

We also define the effective tunneling into and from an invariant region $\Omega_k \subset \mathcal{M}$ from time t_0 to time t as

$$\mathcal{T}_{\Omega_k}(t,t_0) = \mathcal{V}_{\Omega_k}(t) - \mathcal{V}_{\Omega_k}(t_0). \tag{21}$$

Note that if $\mathcal{M} = \bigcup_k \Omega_k$ with $\Omega_k \cap \Omega_{k'} = \emptyset$ for all $k \neq k'$, as shown in Fig. 2, then $\sum_k \mathcal{T}_{\Omega_k}(t,t_0) = 0$ for any time t. If $\mathcal{T}_{\Omega_k}(t,t_0) > 0$, there exists an effective tunneling towards the region Ω_k, while if $\mathcal{T}_{\Omega_k}(t,t_0) < 0$, it indicates the occurrence of an effective tunneling away from this region.

The third definition needed for our analysis is the mean effective tunneling over the invariant region Ω_k from time t_0 to time t, which is written as

$$\overline{\mathcal{T}_{\Omega_k}(t,t_0)} = \frac{1}{t-t_0}\int_{t_0}^{t} d\tau\, \mathcal{T}_{\Omega_k}(t,t_0). \tag{22}$$

In the following two sections we present our results for the analysis of quantum tunneling when Δ/K takes even or odd values. For the initial states considered in Sec. III A, we are able to dynamically determine the values of Δ/K associated with avoided crossings, and for the initial states in Sec. III B we pinpoint the values of Δ/K associated with real crossings.

A. Dynamical identification of the parameters for avoided crossings

We start the study with initial states that have energy between the two ESQPTs, in the energy region of crossings $E_{\mathrm{ESQPT}}^{(\mathrm{III})} < E_\Psi < E_{\mathrm{step}}^{(\mathrm{III})}$.

1. Initial coherent state

In Fig. 6 we consider as initial state $|\Psi(0)\rangle$ coherent states that are initially centered in the region Ω_{out}, as seen in Figs. 6(a1) and 6(b1). The white line in these panels marks the classical separatrix. The evolution of the Husimi function is shown in Figs. 6(a1)–6(a5) for $\Delta/K = 175$ and in Figs. 6(b1)–6(b5) for $\Delta/K = 176$. For the odd case, the state spreads in the region Ω_{out} and visibly tunnels into the classically forbidden region Ω_{in}. This contrasts with the even case, where $|\Psi(t)\rangle$ remains predominantly in Ω_{out}.

The distinctive behavior associated with even and odd Δ/K is quantified with the effective tunneling $\mathcal{T}_{\Omega_k}(t, t_0)$ [Eq. (21)] presented in Figs. 6(c1)–6(c2) for $\Delta/K = 175$ and in Figs. 6(d1)–6(d2) for $\Delta/K = 176$. The tunneling into the regions Ω_{l} and Ω_{r} is minor and analogous for both even and odd Δ/K, as indicated by the very small and quickly saturating positive values of $\mathcal{T}_{\Omega_{\mathrm{l}}}(t, t_0)$ and $\mathcal{T}_{\Omega_{\mathrm{r}}}(t, t_0)$ in Figs. 6(c1) and 6(d1). Tunneling into $\Omega_{\mathrm{l,r}}$ is simply due to the width of the initial coherent state that is not entirely confined to Ω_{out}.

More relevant to the discussion are the results in Figs. 6(c2) and 6(d2) corresponding to the regions Ω_{in} and Ω_{out}. For the odd Δ/K in Fig. 6(c2), $\mathcal{T}_{\Omega_{\mathrm{out}}}(t, t_0)$ [$\mathcal{T}_{\Omega_{\mathrm{in}}}(t, t_0)$] is negative (positive), it decreases (increases) on average, and it does not reach a saturation value for the dimensionless time interval considered. This implies that the state tunnels from Ω_{out} into the classically forbidden region Ω_{in}. In stark contrast with Fig. 6(c2), $\mathcal{T}_{\Omega_{\mathrm{in}}}(t, t_0)$ for the even Δ/K in Fig. 6(d2) is very close to zero, indicating nearly no tunneling into Ω_{in}.

Figure 6(e) depicts the mean effective tunneling $\overline{\mathcal{T}_{\Omega_k}(t, 0)}$ [Eq. (22)] as a function of Δ/K and sums up the results above. This figure provides a tool for the identification of the values of Δ/K where tunneling into the classically prohibited region Ω_{in} is enhanced due to the avoided crossing observed in the spectrum. As evident in the figure, Ω_{in} peaks and Ω_{out} shows troughs only at odd values of Δ/K. However, the results in Fig. 6(e) do not single out the even values of Δ/K as special cases. To identify these values, one needs to resort to other initial states, as described later in Sec. III B.

2. Quench dynamics

A scenario that is often explored in nonequilibrium quantum dynamics, which we consider in this section, is that of quantum quench dynamics, in which the evolution starts with the abrupt change of a parameter of the Hamiltonian [52]. In our case, the ratio Δ/K of the Hamiltonian $\hat{H}$ in Eq. (1) is suddenly modified from Δ_0/K to Δ/K. The initial state is prepared in the ground state of $\hat{H}(\Delta_0/K)$ and it evolves according to $\hat{H}(\Delta/K)$. This provides another example where one can establish through the dynamics that the odd values of Δ/K are associated with avoided crossings.

We fix Δ_0/K and investigate the evolution for different values of Δ/K. Our quench is done from case I with $\Delta_0/K = -6$ and $\epsilon_2/K = 3$ to case III with $\Delta/K > 14$ and $\epsilon_2/K = 3$. For our choices, the Husimi function of the initial state is at the center of the phase space, predominantly in the region Ω_{in}, as seen in Figs. 7(a1)–7(a4). Notice that as Δ/K increases, the area within the separatrix of the first ESQPT [white lines in Figs. 7(a1)–7(a4)] grows, causing the initial state to be better confined within Ω_{in}.

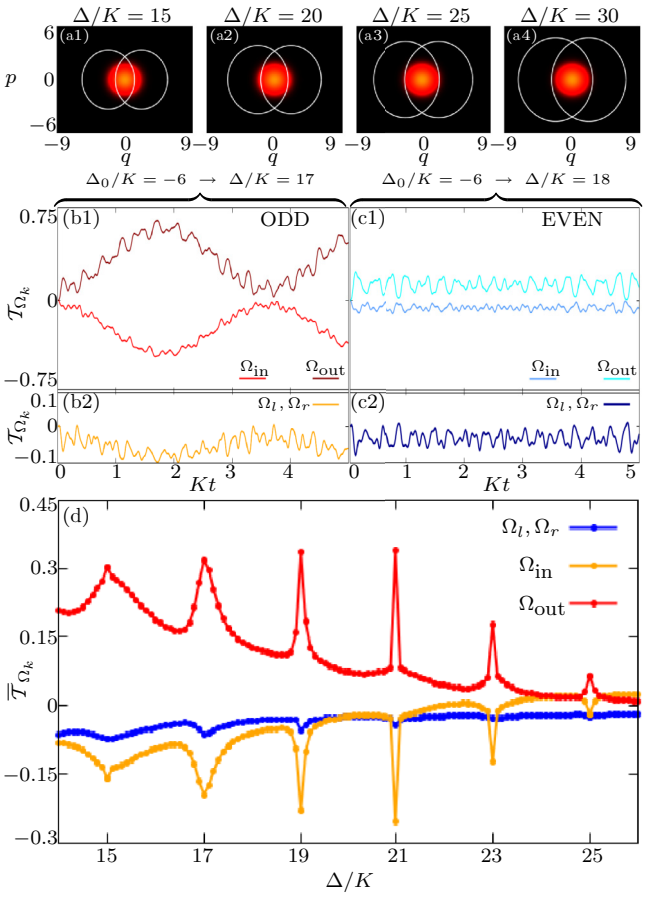

FIG. 7. (a1)–(a4) Husimi function for the ground state of $\hat{H}(\Delta_0/K = -6)$ in the phase space of $H_{\mathrm{cl}}(\Delta/K)$. The effective tunneling is shown after (b1)–(b2) quenching from Δ_0/K to an odd Δ/K and (c1)–(c2) quenching from Δ_0/K to an even Δ/K. (d) Mean effective tunneling after the quench as a function of the parameter Δ/K is obtained for $Kt \in [0, 20]$. In all panels $\epsilon_2/K = 3$.

In Figs. 7(b1)–7(b2) and 7(c1)–7(c2) we show the results of the effective tunneling after the quench to $\Delta/K = 17$ and 18, respectively. For odd Δ/K, the tunneling from Ω_{out} to Ω_{in} in Fig. 7(b1) is significant and more enhanced than in the case of the coherent state in Fig. 6(c2). We see an oscillatory behavior associated with the periodic tunneling between the two regions, while $\mathcal{T}_{\Omega_{\mathrm{l}},\Omega_{\mathrm{r}}}$ in Fig. 7(b2) remains close to zero. In contrast, for even Δ/K, the initial state stays mostly confined to Ω_{in}, as confirmed by the values of $\mathcal{T}_{\Omega_{\mathrm{in}},\Omega_{\mathrm{out}}}$ in Fig. 7(c1) and $\mathcal{T}_{\Omega_{\mathrm{l}},\Omega_{\mathrm{r}}}$ in Fig. 7(c2), which fluctuate close to zero.

Comparing Figs. 6(c2) and 7(b1), one sees that the dynamics is slower for the latter. This is expected, because the energy of the initial state in Fig. 6 is higher than in Fig. 7.

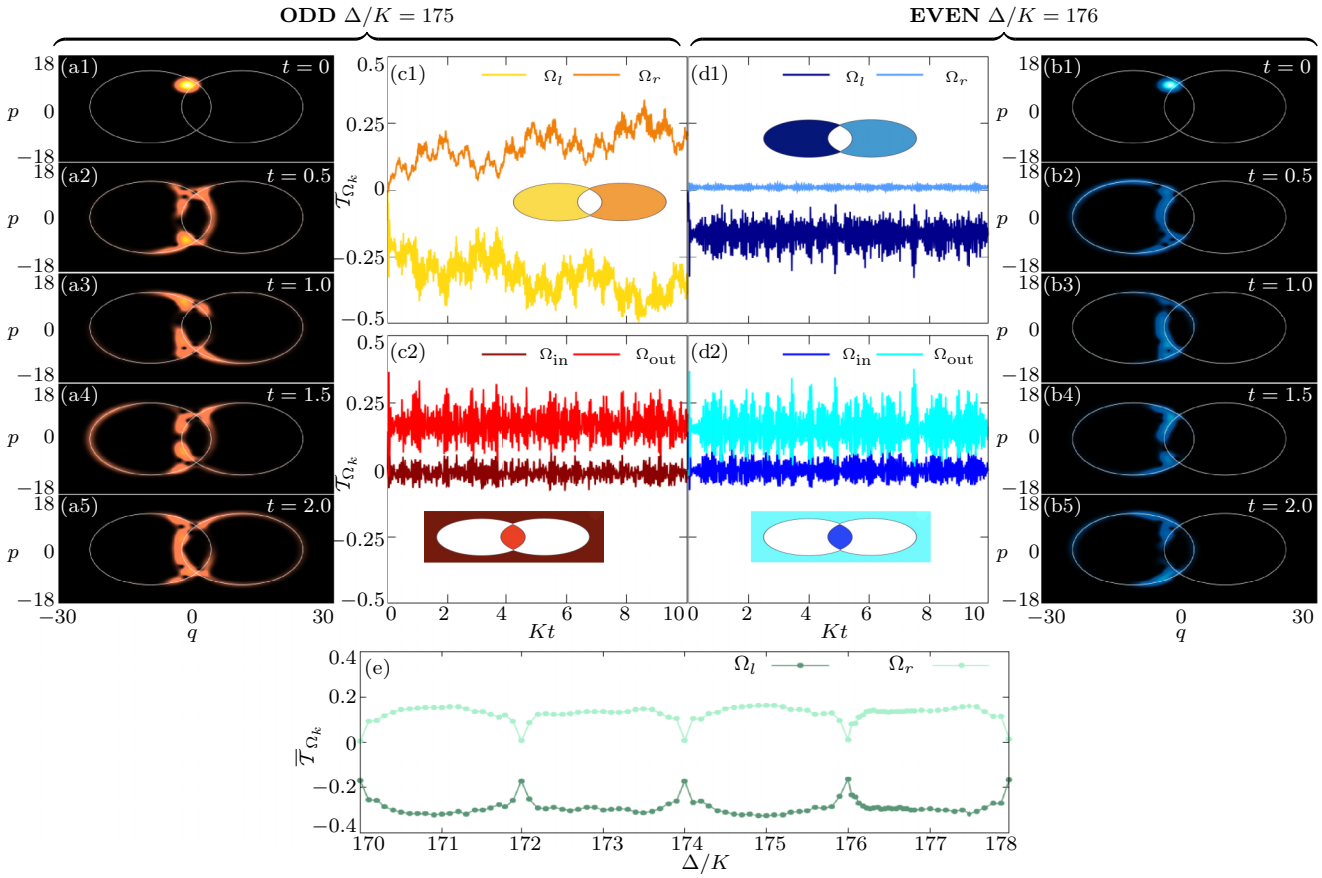

FIG. 8. Evolution of the Husimi function $\mathcal{Q}^{(q,p)}_{\Psi(t)}$ for a coherent state initially centered in the region $\Omega_{\rm l}$ for (a1)–(a5) $\Delta/K = 175$ and (b1)–(b5) $\Delta/K = 176$. The white solid line in these panels indicates the separatrix associated with the hyperbolic fixed points at the energy of the first ESQPT. The energy of the initial coherent state is below the first-ESQPT energy. The results for the effective tunneling $\mathcal{T}_{\Omega_k}$ as a function of dimensionless time are shown in (c1) and (d1) for the regions $\Omega_{\rm l}$ and $\Omega_{\rm r}$ and in (c2) and (d2) for the regions $\Omega_{\rm in}$ and $\Omega_{\rm out}$, for (c1)–(c2) $\Delta/K = 175$ and (d1)–(d2) $\Delta/K = 176$. (e) The mean effective tunneling $\overline{\mathcal{T}_{\Omega_k}(t,0)}$ as a function of the parameter Δ/K is obtained for $Kt \in [0, 10]$. In all panels $\epsilon_2/K = 5$.

Similarly to the analysis in Fig. 6(e), the results for the mean effective tunneling in Fig. 7(d) corroborate the presence of avoided crossings, and thus enhanced tunneling, for odd values of Δ/K. We note that the computation of $\overline{\mathcal{T}_{\Omega_k}(t,0)}$ in Fig. 7(d) is done using the dimensionless time interval $Kt \in [0, 20]$ for all values of Δ/K presented. However, as Δ/K increases and the initial state becomes more deeply confined to $\Omega_{\rm in}$ [cf. Figs. 7(a1)–7(a4)], tunneling takes longer, which explains why the peaks in Fig. 7(d) decrease for larger Δ/K.

B. Dynamical identification of the parameters for real crossings

In Fig. 6(e) $\overline{\mathcal{T}_{\Omega_{\rm in}}(t,0)}$ and $\overline{\mathcal{T}_{\Omega_{\rm out}}(t,0)}$ get closest to zero when Δ/K is even, but there is no particular feature at these points that could indicate anything special about the even values. In this section we show that one can single out those special even values of Δ/K by studying the dynamics for initial coherent states centered in either $\Omega_{\rm l}$ or $\Omega_{\rm r}$ and placed very close to one of the hyperbolic points.

Figure 8 is analogous to Fig. 6, but now for an initial coherent state centered in $\Omega_{\rm l}$ and close to the hyperbolic point r_1^+. The Husimi function for odd Δ/K in Figs. 8(a1)–8(a5) penetrates into the $\Omega_{\rm r}$ region, as confirmed by Fig. 8(c1), where $\mathcal{T}_{\Omega_{\rm l}}$ is negative and $\mathcal{T}_{\Omega_{\rm r}}$ is positive. In contrast, for even Δ/K, the region $\Omega_{\rm r}$ remains mostly empty, as observed in Figs. 8(b1)–8(b5) and verified with Fig. 8(d1). The purpose of Figs. 8(c2) and 8(d2) is simply to show that in both cases part of the Husimi function can be found in $\Omega_{\rm out}$.

The different behaviors for even and odd values of Δ/K reflect the properties of the spectrum. The initial states in Fig. 8 have energy below but very close to $E^{\rm (III)}_{\rm ESQPT}$. They are in the energy region where the degeneracy between the eigenstates in the negative and positive parity sectors gets lifted everywhere, except for the points where Δ/K is even, as illustrated with arrows in Fig. 3(b). This means that one can have tunneling from $\Omega_{\rm l}$ to $\Omega_{\rm r}$ for any value of Δ/K, including odd values, as on the left side of Fig. 8, but excluding even values, as in Figs. 8(a1)–8(a5) and Figs. 8(c1)–8(c2), but excluding even values, as in Figs. 8(b1)–8(b5) and Figs. 8(d1)–8(d2).

We can use the mean effective tunneling presented in Fig. 8(e) to determine, directly through the dynamics the values of Δ/K where real crossings occur in the spectrum. One see that $\overline{\mathcal{T}_{\Omega_{\rm l}}(t,0)}$ exhibits peaks and $\overline{\mathcal{T}_{\Omega_{\rm r}}(t,0)}$ exhibits troughs at even values of Δ/K, indicating the suppression of tunneling from the left to the right region at these points.

Our analysis in Fig. 8(e) confirms experimental results obtained in Ref. [34] for an initial state prepared in one of the wells and with energy close to the ESQPT. By measuring which-well information after different intervals of time, peaks are found in the relaxation time of this dissipative system for even values of Δ/K, indicating cancellation of tunneling.

IV. DISCUSSION

We carried out a detailed analysis of the spectrum and quantum tunneling of the static effective Hamiltonian of a squeeze-driven Kerr oscillator. This is a model with a long history [38,53–55], which has only recently been realized experimentally in the quantum regime [31,34,56]. The control parameters considered here and in Ref. [34] are the harmonic coefficient Δ, the nonlinear Kerr coefficient K, and the squeezing coefficient ϵ_2.

We focused on the parameters values that characterize what we called case III, where $\Delta/K > 2\epsilon_2/K$ and the density of states exhibits two excited-state quantum phase transitions, one associated with a logarithmic peak and the other with a step discontinuity, as described in Sec. II. For even values of Δ/K, real crossings occur for all energy levels, from the ground-state energy up to the energy of the second ESQPT at the step discontinuity. In the intermediate-energy regime enclosed by the two ESQPTs, additional avoided crossings emerge for odd values of Δ/K. The condition for the real and avoided crossings in this intermediate energy region was derived from the Einstein-Brillouin-Keller quantization rule. They are related to the existence of pairs of trajectories with the same energy, each trajectory lying in a different invariant region of the classical phase space and covering a different phase-space area.

In Sec. III we proposed to use tunneling dynamics to uncover the features of the spectrum that arise in the intermediate-energy region between the two ESQPTs. We were able to determine, directly from the dynamics, the special values of Δ/K related to the energy crossings. This may inspire similar analysis of other driven or nondriven systems described by Hamiltonians comparable to the one considered here.

Our numerical protocol employed the effective flux of the Husimi volume to monitor and quantify the dynamics of an evolved state in specific regions of phase space. We explored two scenarios: quench dynamics and dynamics initiated with a coherent state. Quantum tunneling was controlled by varying Δ/K. It was enhanced for odd values of Δ/K, as we showed for initial states with energy between the ESQPTs, and suppressed for even values of Δ/K, as shown for initial states with energy slightly below the first ESQPT.

We close this paper with a general discussion in three paragraphs.

This first paragraph concerns the generality of our results. Based on our analysis and reviewing the previous literature on one-body systems that exhibit energy crossings, we formulated the following conjecture. For systems with one effective degree of freedom, a sufficient condition for the emergence of energy crossings in an intermediate region of the spectrum and only for specific values of the Hamiltonian parameters is that the DOS exhibits at least a local logarithmic divergence and a local step discontinuity, which must be consecutive and can appear in any order. The crossings are observed at energies between these two transitions. Correspondingly, in the underlying classical system, there should be at least two local stationary points in the phase space, a local hyperbolic point and a local center point, which are related to the logarithmic divergence and the step discontinuity in the DOS, respectively.

This second paragraph links our findings with current experiments. The results for tunneling involving initial states below (but very close to) the first ESQPT paralleled experimental results obtained in [34]. In the experiment, a localized state was prepared at the bottom of one of the wells and the activation lifetime for the system to thermalize in between the wells due to dissipation [19,21] was measured. The incoherent lifetime signal showed peaks that correspond to even values of Δ/K. Our Fig. 8(e) showed (inverted) tunneling peaks at the same locations. It thus suggests that the timescale for incoherent flipping between wells is ruled by the tunneling properties of the state close to the ESQPT. From our observations and those made in [31,34], we conjecture that the interwell incoherent dynamics in between wells is determined, only if in part, by the nature of the ESQPT mediating the activation. This conjecture is consistent with the experimental observations made in [31] and with the semiclassical and quantum dissipative theory developed therein regarding the Arrhenius law, where the incoherent thermalization dynamics between the wells also mirrors the Hamiltonian spectrum at the level of the ESQPT. Up to now, the theoretical understanding of the incoherent interwell thermalization dynamics in the driven Kerr oscillator has focused on the engineering of the ground state. Our conjecture suggests the importance of the analysis of the dynamics in the vicinity of ESQPTs. Overall, these findings contribute to the theory of thermal activation in the quantum regime [19,57] and to the engineering of autonomously error-protected bosonic qubits [31,34,55,56,58].

This third and last paragraph discusses a potential application of our studies. Experimental systems described by the model Hamiltonian that we considered can serve as a simulation platform of molecular systems, offering control over the strength of interactions that regulate tunneling and nonadiabatic dynamics at avoided crossings and therefore the product yields of reactions. In particular, photochemical reactions are often regulated by real and avoided crossings of electronic excited states, as observed in a wide range of systems, including the photodissociation and geminate recombination of molecules in solution [59], the interfacial electron transfer at functionalized semiconductor interfaces of dye-sensitized solar cells [60], or the photoinduced dynamics of interconversion of chromophores in biological environments [61].

ACKNOWLEDGMENTS

This research was supported by the NSF CCI grant (Award No. 2124511). F.P.-B. is grateful for funding from the European Union's Horizon 2020 research and innovation program under Grant No. PID2019-104002GB-C21 funded by MCIN/AEI/10.13039/501100011033 and, as appropriate, by ERDF A way of making Europe, by the European Union, or

by the European Union Next Generation EU/PRTR. Computing resources supporting this work were partially provided by the CEAFMC and Universidad de Huelva High Performance Computer located on the Campus Universitario el Carmen and funded by FEDER/MINECO Project No. UNHU-15CE-2848.

[1] F. Hund, Zur deutung der molekelspektren. I, Z. Phys. **40**, 742 (1927).
[2] F. Hund, Zur deutung der molekelspektren. III, Z. Phys. **43**, 805 (1927).
[3] L. Nordheim, Zur theorie der thermischen emission und der reflexion von elektronen an metallen, Z. Phys. **46**, 833 (1928).
[4] R. W. Gurney and E. U. Condon, Quantum mechanics and radioactive disintegration, Phys. Rev. **33**, 127 (1929).
[5] G. Gamow, The quantum theory of nuclear disintegration, Nature (London) **122**, 805 (1928).
[6] H. W. Kroto, *Molecular Rotation Spectra* (Wiley, London, 1975).
[7] C. H. Townes and A. L. Schawlow, *Microwave Spectroscopy* (McGraw-Hill, New York, 1955).
[8] R. P. Feynman, R. B. Leighton, and M. Sands, *The Feynman Lectures on Physics* (Addison-Wesley, Reading, 1966).
[9] J. Meisner and J. Kästner, Atom tunneling in chemistry, Angew. Chem. Int. Ed. **55**, 5400 (2016).
[10] P. R. Schreiner, Quantum mechanical tunneling is essential to understanding chemical reactivity, Trends Chem. **2**, 980 (2020).
[11] R. Wild, M. Nötzold, M. Simpson, T. D. Tran, and R. Wester, Tunnelling measured in a very slow ion-molecule reaction, Nature (London) **615**, 425 (2023).
[12] S. Fölling, S. Trotzky, P. Cheinet, M. Feld, R. Saers, A. Widera, T. Müller, and I. Bloch, Direct observation of second-order atom tunnelling, Nature (London) **448**, 1029 (2007).
[13] M. H. Devoret, J. M. Martinis, and J. Clarke, Measurements of Macroscopic Quantum Tunneling out of the Zero-Voltage State of a Current-Biased Josephson Junction, Phys. Rev. Lett. **55**, 1908 (1985).
[14] J. H. Xu, J. L. Shen, J. H. Miller, and C. S. Ting, Superconducting Pairing Symmetry and Josephson Tunneling, Phys. Rev. Lett. **73**, 2492 (1994).
[15] G.-R. Feng, Y. Lu, L. Hao, F.-H. Zhang, and G.-L. Long, Experimental simulation of quantum tunneling in small systems, Sci. Rep. **3**, 2232 (2013).
[16] A. P. Dmitriev, M. I. Dyakaonov, and A. F. Ioffe, Activated and tunneling transitions between the two forced-oscillation regimes of an anharmonic oscillator, Zh. Eksp. Teor. Fiz. **90**, 1430 (1986) [Sov. Phys. JETP **63**, 838 (1986)].
[17] F. Grossmann, T. Dittrich, P. Jung, and P. Hänggi, Coherent Destruction of Tunneling, Phys. Rev. Lett. **67**, 516 (1991).
[18] F. Großmann and P. Hänggi, Localization in a driven two-level dynamics, Europhys. Lett. **18**, 571 (1992).
[19] M. Marthaler and M. I. Dykman, Switching via quantum activation: A parametrically modulated oscillator, Phys. Rev. A **73**, 042108 (2006).
[20] M. Marthaler and M. I. Dykman, Quantum interference in the classically forbidden region: A parametric oscillator, Phys. Rev. A **76**, 010102(R) (2007).
[21] M. Dykman, *Fluctuating Nonlinear Oscillators: From Nanomechanics to Quantum Superconducting Circuits* (Oxford University Press, Oxford, 2012).
[22] G. J. Milburn, J. Corney, E. M. Wright, and D. F. Walls, Quantum dynamics of an atomic Bose-Einstein condensate in a double-well potential, Phys. Rev. A **55**, 4318 (1997).
[23] A. J. Leggett, Bose-Einstein condensation in the alkali gases: Some fundamental concepts, Rev. Mod. Phys. **73**, 307 (2001).
[24] S. Zöllner, H.-D. Meyer, and P. Schmelcher, Few-Boson Dynamics in Double Wells: From Single-Atom to Correlated Pair Tunneling, Phys. Rev. Lett. **100**, 040401 (2008).
[25] S. Zöllner, H.-D. Meyer, and P. Schmelcher, Tunneling dynamics of a few bosons in a double well, Phys. Rev. A **78**, 013621 (2008).
[26] S. Hunn, K. Zimmermann, M. Hiller, and A. Buchleitner, Tunneling decay of two interacting bosons in an asymmetric double-well potential: A spectral approach, Phys. Rev. A **87**, 043626 (2013).
[27] S. M. H. Halataei and A. J. Leggett, Tunnel splitting in asymmetric double well potentials: An improved WKB calculation, arXiv:1703.05758.
[28] D. J. Nader, C. A. González-Rodríguez, and S. Lerma-Hernández, Avoided crossings and dynamical tunneling close to excited-state quantum phase transitions, Phys. Rev. E **104**, 064116 (2021).
[29] R. Harris, M. W. Johnson, S. Han, A. J. Berkley, J. Johansson, P. Bunyk, E. Ladizinsky, S. Govorkov, M. C. Thom, S. Uchaikin, B. Bumble, A. Fung, A. Kaul, A. Kleinsasser, M. H. S. Amin, and D. V. Averin, Probing Noise in Flux Qubits via Macroscopic Resonant Tunneling, Phys. Rev. Lett. **101**, 117003 (2008).
[30] N. E. Frattini, U. Vool, S. Shankar, A. Narla, K. M. Sliwa, and M. H. Devoret, 3-wave mixing Josephson dipole element, Appl. Phys. Lett. **110**, 222603 (2017).
[31] N. E. Frattini, R. G. Cortiñas, J. Venkatraman, X. Xiao, Q. Su, C. U. Lei, B. J. Chapman, V. R. Joshi, S. M. Girvin, R. J. Schoelkopf, S. Puri, and M. H. Devoret, The squeezed Kerr oscillator: Spectral kissing and phase-flip robustness, arXiv:2209.03934.
[32] S. Pilatowsky-Cameo, J. Chávez-Carlos, M. A. Bastarrachea-Magnani, P. Stránský, S. Lerma-Hernández, L. F. Santos, and J. G. Hirsch, Positive quantum Lyapunov exponents in experimental systems with a regular classical limit, Phys. Rev. E **101**, 010202(R) (2020).
[33] J. Chávez-Carlos, T. L. M. Lezama, R. G. Cortiñas, J. Venkatraman, M. H. Devoret, V. S. Batista, F. Pérez-Bernal, and L. F. Santos, Spectral kissing and its dynamical consequences in the squeeze-driven Kerr oscillator, npj Quantum Inf. **9**, 76 (2023).
[34] J. Venkatraman, R. G. Cortinas, N. E. Frattini, X. Xiao, and M. H. Devoret, A driven quantum superconducting circuit with multiple tunable degeneracies, arXiv:2211.04605.
[35] A. Einstein, Zum quantensatz von Sommerfeld und Epstein, Verh. Dtsch. Phys. Ges. **19**, 82 (1917).
[36] L. Brillouin, Remarques sur la mécanique ondulatoire, J. Phys. Radium **7**, 353 (1926).

[37] J. B. Keller, Corrected Bohr-Sommerfeld quantum conditions for non-separable systems, Ann. Phys. (NY) **4**, 180 (1958).
[38] Y. Zhang and M. I. Dykman, Preparing quasienergy states on demand: A parametric oscillator, Phys. Rev. A **95**, 053841 (2017).
[39] F. Iachello, R. G. Cortiñas, F. Pérez-Bernal, and L. F. Santos, Symmetries of the squeezed Kerr oscillator (unpublished).
[40] M. Caprio, P. Cejnar, and F. Iachello, Excited state quantum phase transitions in many-body systems, Ann. Phys. (NY) **323**, 1106 (2008).
[41] P. Stránský and P. Cejnar, Classification of excited-state quantum phase transitions for arbitrary number of degrees of freedom, Phys. Lett. A **380**, 2637 (2016).
[42] P. Cejnar, P. Stránský, M. Macek, and M. Kloc, Excited-state quantum phase transitions, J. Phys. A: Math. Theor. **54**, 133001 (2021).
[43] I. García-Mata, E. Vergini, and D. A. Wisniacki, Impact of chaos on precursors of quantum criticality, Phys. Rev. E **104**, L062202 (2021).
[44] M. C. Gutzwiller, *Chaos in Classical and Quantum Mechanics* (Springer, New York, 1990).
[45] E. Grigoriou and C. Navarrete-Benlloch, Signatures of a quantum phase transition on a single-mode bosonic model, arXiv:2303.12894.
[46] J. von Neumann and E. P. Wigner, Über merkwürdige diskrete eigenwerte, Z. Phys. **30**, 465 (1929).
[47] Y. N. Demkov and P. B. Kurasov, Von Neumann–Wigner theorem: Level repulsion and degenerate eigenvalues, Theor. Math. Phys. **153**, 1407 (2007).
[48] D. Khuat-duy and P. Leboeuf, Multiresonance tunneling effect in double-well potentials, Appl. Phys. Lett. **63**, 1903 (1993).
[49] E. M. Graefe and H. J. Korsch, Semiclassical quantization of an N-particle Bose-Hubbard model, Phys. Rev. A **76**, 032116 (2007).
[50] L. F. Santos and F. Pérez-Bernal, Structure of eigenstates and quench dynamics at an excited-state quantum phase transition, Phys. Rev. A **92**, 050101(R) (2015).
[51] D. Villaseñor, S. Pilatowsky-Cameo, M. A. Bastarrachea-Magnani, S. Lerma-Hernández, and J. G. Hirsch, Quantum localization measures in phase space, Phys. Rev. E **103**, 052214 (2021).
[52] A. Mitra, Quantum quench dynamics, Annu. Rev. Condens. Matter Phys. **9**, 245 (2018).
[53] B. Wielinga and G. J. Milburn, Quantum tunneling in a Kerr medium with parametric pumping, Phys. Rev. A **48**, 2494 (1993).
[54] P. T. Cochrane, G. J. Milburn, and W. J. Munro, Macroscopically distinct quantum-superposition states as a bosonic code for amplitude damping, Phys. Rev. A **59**, 2631 (1999).
[55] S. Puri, S. Boutin, and A. Blais, Engineering the quantum states of light in a Kerr-nonlinear resonator by two-photon driving, npj Quantum Inf. **3**, 18 (2017).
[56] A. Grimm, N. E. Frattini, S. Puri, S. O. Mundhada, S. Touzard, M. Mirrahimi, S. M. Girvin, S. Shankar, and M. H. Devoret, Stabilization and operation of a Kerr-cat qubit, Nature (London) **584**, 205 (2020).
[57] P. Hänggi, P. Talkner, and M. Borkovec, Reaction-rate theory: Fifty years after Kramers, Rev. Mod. Phys. **62**, 251 (1990).
[58] D. Ruiz, R. Gautier, J. Guillaud, and M. Mirrahimi, Two-photon driven Kerr quantum oscillator with multiple spectral degeneracies, Phys. Rev. A **107**, 042407 (2023).
[59] V. S. Batista and D. F. Coker, Nonadiabatic molecular dynamics simulation of photodissociation and geminate recombination of I_2 liquid xenon, J. Chem. Phys. **105**, 4033 (1996).
[60] S. G. Abuabara, L. G. C. Rego, and V. S. Batista, Influence of thermal fluctuations on interfacial electron transfer in functionalized TiO_2 semiconductors, J. Am. Chem. Soc. **127**, 18234 (2005).
[61] X. Chen and V. S. Batista, The MP/SOFT methodology for simulations of quantum dynamics: Model study of the photoisomerization of the retinyl chromophore in visual rhodopsin, J. Photochem. Photobiol. A **190**, 274 (2007).